Research Paper

Oxysterol Signatures Distinguish Age-Related Macular Degeneration from Physiologic Aging

Jonathan B. Lin [a,b,1], Abdoulaye Sene [a,1], Andrea Santeford [a], Hideji Fujiwara [c,d], Rohini Sidhu [c,d], Marianne M. Ligon [e], Vikram A. Shankar [a], Norimitsu Ban [a], Indira U. Mysorekar [e,f], Daniel S. Ory [c,d], Rajendra S. Apte [a,c,d,g,*]

[a] Department of Ophthalmology & Visual Sciences, Washington University School of Medicine, St. Louis, MO, USA
[b] Neuroscience Graduate Program, Division of Biology and Biomedical Sciences, Washington University School of Medicine, St. Louis, MO, USA
[c] Diabetic Cardiovascular Disease Center, Washington University School of Medicine, St. Louis, MO, USA
[d] Department of Medicine, Washington University School of Medicine, St. Louis, MO, USA
[e] Department of Pathology and Immunology, Washington University School of Medicine, St. Louis, MO, USA
[f] Center for Reproductive Health Sciences, Department of Obstetrics and Gynecology, Washington University School of Medicine, St. Louis, MO, USA
[g] Department of Developmental Biology, Washington University School of Medicine, St. Louis, MO, USA

ARTICLE INFO

ABSTRACT

Macrophage aging is pathogenic in numerous diseases, including age-related macular degeneration (AMD), a leading cause of blindness in older adults. Although prior studies have explored the functional consequences of macrophage aging, less is known about its cellular basis or what defines the transition from physiologic aging to disease. Here, we show that despite their frequent self-renewal, macrophages from old mice exhibited numerous signs of aging, such as impaired oxidative respiration. Transcriptomic profiling of aged murine macrophages revealed dysregulation of diverse cellular pathways, especially in cholesterol homeostasis, that manifested in altered oxysterol signatures. Although the levels of numerous oxysterols in human peripheral blood mononuclear cells and plasma exhibited age-associated changes, plasma 24-hydroxycholesterol levels were specifically associated with AMD. These novel findings demonstrate that oxysterol levels can discriminate disease from physiologic aging. Furthermore, modulation of cholesterol homeostasis may be a novel strategy for treating age-associated diseases in which macrophage aging is pathogenic.

1. Introduction

Age-related macular degeneration (AMD) is a leading cause of blindness in adults over 50 years of age in industrialized nations [1]. Early AMD is characterized by the presence of lipoproteinaceous deposits or drusen under the retinal pigment epithelium (RPE) and/or thickening of Bruch's membrane. Although early AMD is not always associated with vision loss, it is a major risk factor for progression to one of two forms of advanced AMD: a dry form, characterized by death of RPE cells called geographic atrophy (GA) that eventually leads to death of overlying photoreceptors, or wet (neovascular) form, characterized by abnormal vascular proliferation underneath the retina called choroidal neovascularization (CNV). While both advanced dry and wet AMD can cause vision loss, wet AMD accounts for a significant fraction of the vision loss associated with AMD [2] and can often be acute and catastrophic.

The current mainstay therapies for wet AMD focus on combating abnormal angiogenesis by blocking vascular endothelial growth factor (VEGF) with targeted anti-VEGF agents. These treatments stabilize disease in a majority of patients and significantly improve visual outcomes in 30–40% of wet AMD patients [3–5]. However, these therapies often require frequent visits for repeated intraocular injections, which places a significant burden on patients and caregivers [6]. Moreover, repeated intravitreal injections are also associated with risks of their own, such as infection, scleral thinning, and long-term visual acuity loss due to continued atrophy of the RPE and photoreceptors [3, 7]. Perhaps more importantly, anti-VEGF agents do not address the pathophysiology that causes wet AMD [8]. Therefore, there is need for further research to clarify the molecular and cellular mechanisms involved in the transition from physiologic aging to AMD and to understand the pathogenesis underlying the progression from early to wet AMD, which may lead to novel strategies for targeted intervention.

In the past few decades, we and others have demonstrated that macrophages, key cells of the innate immune system, play important roles

* Corresponding author at: 660 South Euclid Avenue, Box 8096, St. Louis, MO 63110, USA.
E-mail address: apte@vision.wustl.edu (R.S. Apte).
[1] These authors contributed equally to this work.

in the pathogenesis of wet AMD [9–12]. Moreover, it has become increasingly clear that the ability of macrophages to polarize to different activation states is an important factor affecting whether macrophages promote health or disease [13]. Depending on dynamic tissue signals and the surrounding micro-environment, macrophages can polarize to a classical pro-inflammatory (M1-like) phenotype, an alternative anti-inflammatory (M2-like) phenotype, or some intermediate between these two extremes [14]. To further complicate matters, the identity of the specific activators that cause macrophage polarization may also affect the macrophage phenotype [15].

Previously, we reported that aged macrophages tend to skew to the anti-inflammatory M2-like phenotype and are less able to inhibit abnormal angiogenesis [16]. Furthermore, aged macrophages exhibit both impairments in cholesterol efflux [17] and abnormalities in IL-10 and downstream STAT3 signaling pathways that contribute to this age-associated drift towards M2-like polarization [18]. These age-associated impairments in cholesterol efflux and other lipid-related pathways may have mechanistic consequences in disease pathogenesis [19]. This possibility is supported by the fact that polymorphisms in lipid-related genes, such as hepatic lipase (LIPC), ATP-binding cassette transporter member 1 (ABCA1), and cholesterol ester transfer protein (CETP), are associated with advanced AMD [20]. Moreover, drusen, a clinical feature of early AMD, are lipid-rich, further supporting our hypothesis that dysregulated lipid homeostasis contributes to AMD. Despite these advances, the global programmatic changes that occur during macrophage aging need further elucidation. It is also unclear what subset of these changes are associated with physiologic aging or are pathologic and contribute to age-associated disease.

In this study, we sought to delineate the cellular pathways involved in macrophage aging and identify potential markers that may distinguish age-associated changes that are physiologic versus those that promote age-associated disease. Our results suggest that impaired cholesterol homeostasis in macrophages is a central process perturbed during aging and that these changes lead to alterations in oxysterol signatures that can distinguish AMD from physiologic aging. These findings may allow physicians to monitor progression of disease with quantifiable serum markers and may potentially lead to novel therapeutic strategies not only for AMD but also for other age-associated diseases in which alternatively-activated macrophages are pathogenic.

2. Materials and Methods

2.1. Animals

All animal experiments were approved by the Institutional Animal Care and Use Committee (IACUC) and performed in accordance with the Washington University School of Medicine Animal Care and Use guidelines. We obtained old (i.e., ~18-month-old), female wild-type C57BL/6J mice from the National Institute on Aging (Bethesda, MD) and compared them to strain-matched young (i.e., ~3-month-old), female wild-type C57BL/6J controls. We harvested peritoneal macrophages five days after elicitation with a 2-ml intraperitoneal injection of 4% thioglycollate broth (Sigma-Aldrich, St. Louis, MO). We harvested splenic macrophages by performing positive magnetic cell separation with the PE selection kit (Stem Cell Technologies) and PE anti-F4/80 monoclonal antibody (clone: BM8; eBioscience, Waltham, MA), following manufacturer's instructions. We cultured peritoneal and splenic macrophages in Gibco™ RPMI 1640 medium (Thermo Fisher Scientific, Waltham, MA) supplemented with 10% fetal bovine serum (FBS; Atlanta Biologicals, Flowery Branch, GA) and 1% penicillin-streptomycin (Thermo Fisher Scientific). When indicated, we treated macrophages with 25 or 50 μg/ml of oxidized LDL (oxLDL; Alfa Aesar, Haverhill, MA) for 24 h prior to further analysis.

2.2. OCR Measurements

To perform metabolic characterization, we measured the oxygen consumption rate (OCR) of peritoneal macrophages as a surrogate marker for oxidative respiration with the XF96 Extracellular Flux Analyzer (Seahorse Bioscience, North Billerica, MA). In short, we plated peritoneal macrophages in Seahorse XF96 cell culture microplates (Seahorse Bioscience) at 100,000 cells per well. On the morning of the experiment, we washed the cells and replaced the medium with Seahorse assay medium (Seahorse Bioscience) supplemented with 25 mM glucose (Sigma-Aldrich, St. Louis, MO) and 1 mM sodium pyruvate (Thermo Fisher Scientific) and adjusted the pH to 7.4. After incubation in a non-CO_2 incubator at 37 °C for 1 h, we measured OCR at baseline and after sequential treatment with the following chemicals from the Mito Stress Test kit (Seahorse Bioscience): 3 μM oligomycin, 5 μM carbonyl cyanide 4-(trifluoromethoxy) phenylhydrazone (FCCP), and 1 μM rotenone/antimycin A (rot/AA). Each cycle consisted of 2 min of mixing and a 1-min pause, followed by a 5-min measurement period; we repeated each cycle 3–4 times. We normalized the background of all measurements by subtracting the average OCR of each sample after treatment with rot/AA.

2.3. Gene Expression Analysis

We extracted total RNA from peritoneal macrophages with the RNeasy Mini kit (Qiagen) and prepared cDNA with the High-Capacity Reverse Transcription kit (Applied Biosystems), following manufacturer's instructions. We performed quantitative PCR amplification of cDNA using either the TaqMan® probe-based gene expression assay for $p16^{INK4a}$ (Mm00494449_m1; Applied Biosystems) or custom TaqMan® Array Plates (Applied Biosystems) for lipid-related genes with the assays indicated in Supplemental Table S1. In all cases, we used the ΔΔCT method, normalizing to *Actb*, *18sRNA*, *Gapdh*, or the geometric mean of a combination of these endogenous controls.

2.4. Transcriptomic Profiling

We isolated total RNA from peritoneal macrophages with the mirVana kit (Ambion), performed cDNA amplification with the Ovation® Pico kit (NuGEN, San Carlos, CA), and performed target labeling with the Encore® Biotin kit (NuGEN), according to manufacturer's instructions. We then performed whole transcriptome profiling of young and aged peritoneal macrophages using Mouse Gene (MoGene) 1.0 ST arrays processed with Affymetrix Expression Console (v1.3.1.187) at standard settings (RMA background correction, median polish summarization, and quantile normalization) to generate intensity values. We assigned each probeset of the MoGene 1.0 array a detection call of 'mean + 2 × SD' of the negative controls. We performed data quality control to identify potential outliers by principal component analysis (PCA) plot and hierarchical clustering, as well as by quality control (QC) metrics (all probeset RLE means > 0.25) in Expression Console. From this QC, we omitted one sample in the young group. We then filtered data by probeset type ("main" in MoGene 1.0) and by detection call (any probeset without a "detected" call in any of the samples was removed). Any probeset without a gene symbol in the MoGene 1.0 data was also removed. 18,066 MoGene 1.0 probesets (from the total of 35,556) were kept for further analysis. We analyzed the data using the R package "limma" and generated gene lists based on *P*-values and false detection rate (FDR) q-values. We performed gene ontology (GO), pathway map, and interactome analyses with MetaCore™ (Clarivate Analytics, Philadelphia, PA). The microarray data are available at the Gene Expression Omnibus (GEO) at NCBI under accession number GSE111382.

2.5. Flow Cytometry

We plated peritoneal macrophages on untreated Petri dishes and allowed them to adhere overnight. The next morning, we lifted cells by incubating for 5 min in ice-cold Dulbecco's phosphate-buffered saline (DPBS; Thermo Fisher Scientific) without calcium or magnesium and scraping gently. We next filtered cells through a 40 μm cell strainer, washed them with DPBS, and resuspended them in DPBS containing 5% FBS, 10 mM HEPES, 1 mM EDTA, and TruStain fcX™ antibody (BioLegend, San Diego, CA). We stained 10^5 to 10^6 cells with APC anti-mouse CD36 (clone: HM36; BioLegend), PE/Cy7 anti-mouse CD64 (clone: ×54–5/7.1; BioLegend), and PE anti-mouse F4/80 (clone: BM8; eBioscience) antibodies for 20 min on ice. We then washed and resuspended cells in DPBS and acquired data on a BD X-20 or BD LSR II flow cytometer (BD Biosciences, San Jose, CA). We analyzed and visualized data with FlowJo v10.

2.6. Human Subjects

This study was approved by the Human Research Protection Office of Washington University School of Medicine and adhered to the Declaration of Helsinki. We obtained informed consent from all subjects prior to blood collection. To purify peripheral blood mononuclear cells (PBMCs) and plasma, we performed density gradient centrifugation with BD Vacutainer CPT™ Cell Preparation Tubes (Franklin Lakes, NJ), following manufacturer's instructions. We classified patients as no AMD, early AMD, or wet AMD based on established clinical criteria [21]. Early AMD patients had either moderate drusen (>63 μm) or pigment changes in at least one eye but no CNV or GA in either eye at the time of sample collection. Wet AMD patients had CNV in at least one eye at the time of sample collection. We stored all samples at −80 °C until further analysis. To determine the appropriate sample size, we performed an a priori power analysis with G*Power 3.1 [22]. Estimating an effect size d of 0.6 based on pilot experiments, we calculated that we needed 94 subjects with an allocation ratio of 1.5:1 to detect a significant difference between the groups at the two-sided $\alpha = 0.05$ level with 80% power. For the subanalysis, we performed chart review to identify the closest total plasma cholesterol measurement obtained within 3.5 years of the date of sample collection.

2.7. Oxysterol Profiling by LC–MS/MS

We extracted and quantified oxysterol levels from murine peritoneal macrophage pellets, the supernatant of murine peritoneal macrophages, human PBMC pellets, and human plasma samples as previously described [23]. Briefly, we added deuterated oxysterols to the samples as internal standards and then extracted oxysterols with methanol. We derivatized the extracted oxysterols and their internal standards with N,N-dimethylglycinate (DMG) to increase MS sensitivity. We performed oxysterol analysis with a Shimadzu 20 CE HPLC system (Kyoto, Japan) and a LeapPAL autosampler coupled to a tandem mass spectrometer (API 4000; Applied Biosystems) operated in MRM mode. We used positive ion ESI mode for detection of the derivatized oxysterols, injecting study samples in duplicate for data averaging. We conducted data processing with Analyst 1.5.1 (Applied Biosystems) and determined relative levels of each oxysterol by comparing its measurement with that of its corresponding deuterated internal standard. We normalized the murine macrophage oxysterol levels to cell number, murine supernatant levels to volume, human PBMC oxysterol levels to protein content, and human plasma oxysterol levels to volume. To normalize human samples processed on different days, we used one of the patient samples as an internal control.

2.8. Statistics

We performed statistical analysis as indicated in the Figure legends with Prism 5 (GraphPad Software) or SPSS Statistics Version 23 (IBM, Armonk, NY). We assessed the normality of our data graphically and with the Kolmogorov-Smirnov test and used appropriate non-parametric alternatives when necessary. We considered $P < .05$ to be statistically
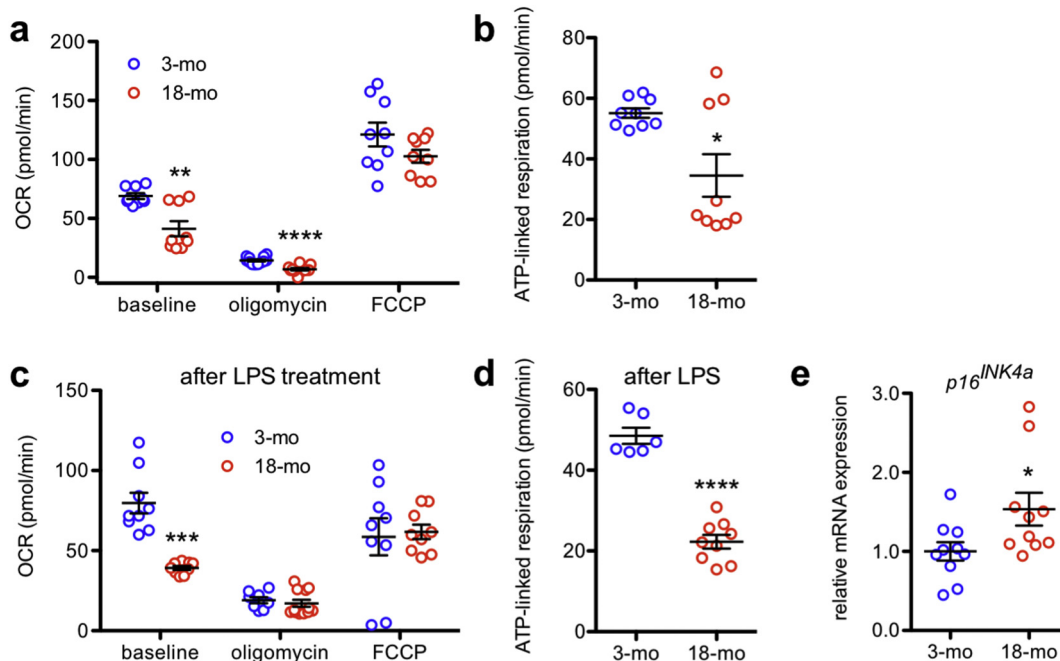

Fig. 1. Peritoneal macrophages from old mice exhibit quantifiable signs of aging. (a) Aged peritoneal macrophages had reduced oxygen consumption rate (OCR) both at baseline ($N = 9$/group; 2-tailed, unpaired Welch's t-test) and in response to oligomycin ($N = 11$–12/group; 2-tailed, unpaired t-test) and significantly reduced ATP-linked respiration (b; $N = 9$/group; 2-tailed, unpaired Welch's t-test). (c) Lipopolysaccharide (LPS)-treated aged peritoneal macrophages also had impaired mitochondrial bioenergetics at baseline ($N = 8$–12/group; 2-tailed, unpaired Welch's t-test) and significantly reduced ATP-linked respiration (d; $N = 6$–9/group; 2-tailed, unpaired t-test) compared to LPS-treated young peritoneal macrophages. (e) Aged peritoneal macrophages had increased mRNA expression of the senescence marker $p16^{INK4a}$ ($N = 10$/group; 2-tailed, unpaired t-test). Open circles depict individual data points; horizontal lines depict mean ± SEM (a-e) (* $P < .05$; ** $P < .01$; *** $P < .001$; **** $P < .0001$).

significant. To model the relationship between PBMC and plasma oxysterol signatures and AMD, we generated binary logistic regression models. Our model included the following predictor variables: age at the time of sample collection, gender, and PBMC/plasma oxysterol levels. For the subanalysis, we generated an additional binary logistic regression model, which included the following predictor variables: age at the time of sample collection, gender, plasma 24-HC levels, and total plasma cholesterol. For all regression models, we assessed fit with the Hosmer-Lemeshow lack-of-fit test and performed diagnostics by examining Cook's distances, leverages, and residual deviances. The final reported models had seven omitted cases based on sensitivity analysis. We checked for problems with collinearity by examining variance inflation factors (VIF). We used an unadjusted alpha of 0.05 for the binary logistic regression.

3. Results

3.1. Peritoneal Macrophages from Old Mice Exhibit Features of Aging

Under steady-state conditions, tissue-resident macrophages are maintained through constant replacement or self-renewal. In many tissues, including the peritoneal cavity, there is extensive replacement of macrophages as quickly as every 3 weeks [24]. Therefore, we sought to determine whether macrophages isolated from old (i.e., 18-month-old) wild-type mice exhibited features of cellular aging when compared to macrophages isolated from young (i.e., 3-month-old) wild-type mice despite this short replenishment cycle.

Mitochondrial dysfunction is a well-established hallmark of aging, and in many tissues, there is an age-dependent decrease in mitochondrial oxygen consumption [25]. To determine whether peritoneal macrophages from old mice exhibit mitochondrial dysfunction, we measured the oxygen consumption rate (OCR) of peritoneal macrophages isolated from 3-month-old and 18-month-old mice. The baseline OCR of peritoneal macrophages from old mice was significantly lower than that of peritoneal macrophages from young mice (Fig. 1a), indicating reduced basal oxidative respiration. Although both young and aged peritoneal macrophages appropriately exhibited a reduction in OCR after treatment with the ATP synthase inhibitor oligomycin, young peritoneal macrophages maintained a somewhat higher residual OCR (Fig. 1a). In contrast, both young and aged peritoneal macrophages demonstrated similar maximal oxidative respiration in response to the uncoupling agent FCCP (Fig. 1a). The difference between the baseline OCR and the OCR after oligomycin treatment represents ATP-linked respiration. Aged peritoneal macrophages exhibited significantly reduced ATP-linked respiration (Fig. 1b), indicating mitochondrial dysfunction.
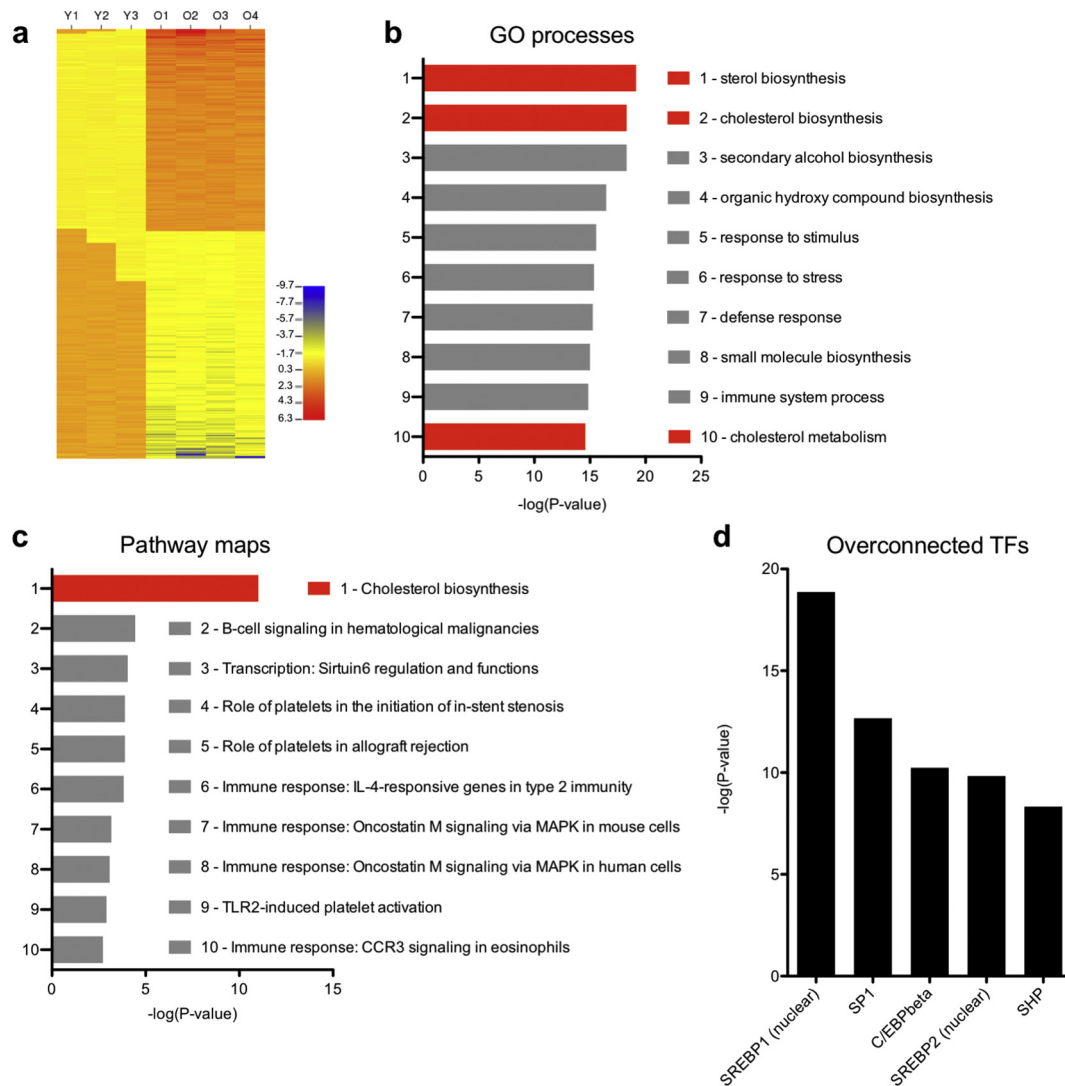

Fig. 2. Transcriptomic profiling of aged peritoneal macrophages. (a) Aged peritoneal macrophages display numerous transcriptomic changes, which suggest perturbations in various gene ontology (GO) processes (b) and pathway maps (c). (d) Interactome analysis revealed numerous overconnected transcription factors (TFs) whose known gene targets were overrepresented in the genes we identified as dysregulated in aged versus young macrophages.

Moreover, previous studies report that exposing macrophages to lipopolysaccharide (LPS) considerably alters their bioenergetic profile [26]. Furthermore, such a metabolic switch is required for macrophage activation and affects subsequent inflammatory status [26–28]. We observed distinct mitochondrial respiratory profiles when comparing young and aged, LPS-treated peritoneal macrophages: aged peritoneal macrophages exhibited a reduced OCR at baseline, despite maintaining similar responses to oligomycin and FCCP (Fig. 1c). Again, aged peritoneal macrophages exhibited significantly reduced ATP-linked respiration (Fig. 1d). Cumulatively, these data demonstrate that mitochondrial oxidative metabolism is considerably impaired in peritoneal macrophages isolated from old mice both at baseline and in response to LPS.

Furthermore, we evaluated the expression of the aging marker $p16^{INK4a}$, which is a known senescence marker in bone marrow-derived macrophages [29] and has been shown to accumulate in rodent and human tissues during aging [30–32]. We found that $p16^{INK4a}$ mRNA expression was significantly elevated in aged peritoneal macrophages compared to young peritoneal macrophages (Fig. 1e). Collectively, these results confirm that despite their constant renewal, peritoneal macrophages from old mice exhibit multiple quantifiable signs of aging, including mitochondrial dysfunction and increased expression of the senescence marker, $p16^{INK4a}$.

3.2. Aged Macrophages Exhibit Impaired Cholesterol Homeostasis

To determine the specific cellular processes that are perturbed in aged macrophages, we profiled the transcriptomes of young and aged macrophages with the GeneChip Mouse Gene 1.0 ST Array (Affymetrix, Santa Clara, CA). We found that 1080 probe sets were significantly differentially expressed in aged versus young macrophages (Fig. 2a; $P <$ .05, FDR < 0.20). The twenty protein-coding genes that were up- or downregulated with the highest fold change in aged versus young macrophages are presented in Table 1. To determine whether the identities of the dysregulated genes were associated with defects in particular pathways or cellular processes, we filtered for genes with a 1.50-fold-change cutoff (22.1%, $N = 239$) and then performed gene ontology (GO) and pathway map analysis with MetaCore™ (Clarivate Analytics, Philadelphia, PA). Of interest, the first, second, and tenth most significant GO processes implicated were sterol biosynthesis, cholesterol biosynthesis, and cholesterol metabolism, respectively (Fig. 2b). Consistently, cholesterol biosynthesis was the most significant pathway map implicated by the altered transcriptomic profile of aged macrophages (Fig. 2c). As expected, the transcriptomic profile of aged macrophages also suggested disruptions in numerous other immune response pathways (Fig. 2c). Overall, these results clearly indicate that cholesterol homeostasis is significantly perturbed during macrophage aging.

Given that numerous genes were dysregulated in aged peritoneal macrophages, we sought to identify candidate transcription factors (TFs) that may regulate the aging process. Therefore, we performed interactome analysis to identify over-connected TFs, which may regulate the observed transcriptomic changes in aged macrophages. Of interest, two of the top five most significantly overconnected TFs were sterol regulatory element-binding protein 1 and 2 (SREBP1/SREBP2; Fig. 2d), which are known master regulators of cholesterol and lipid homeostasis. These two TFs had connectivity ratios of 14.73 and 15.15, respectively, indicating ~15-fold overrepresentation of their known targets. These findings support our assertion that global lipid homeostatic mechanisms are impaired in aged macrophages.

To determine the specific aspects of cholesterol homeostasis that are impaired in aged macrophages, we analyzed the expression profile of 113 lipid-related genes in young and aged macrophages with a custom quantitative PCR array (Applied Biosystems). We were able to detect expression of 86.7% ($N = 98$) of the genes we tested and found that 30 of these 98 cholesterol-related genes (30.6%) had significantly different expression in aged versus young macrophages (Table 2). When we subdivided these lipid-related genes broadly by their cellular function, we observed that they encompassed diverse biological processes, including cholesterol/lipid biosynthesis, elimination, transport, and uptake, among other processes. These findings once again confirmed that aged peritoneal macrophages exhibit global impairments in their ability to maintain cholesterol and lipid homeostasis.

Table 1
Top ten up- and down-regulated genes in aged versus young peritoneal macrophages.

Probeset ID	Gene symbol	Fold change[a]	P-value	FDR
10463355	Scd2	−3.645	0.0007	0.0667
10506571	Dhcr24	−2.522	0.0001	0.0361
10347748	Acsl3	−2.406	0.0003	0.0497
10560702	Ceacam19	−2.266	<0.0001	0.0307
10403413	Idi1	−2.070	0.0018	0.0952
10544273	Clec5a	−1.996	0.0006	0.0634
10482762	Idi1	−1.977	0.0021	0.1006
10420668	Mir15a	−1.969	0.0016	0.0924
10424349	Sqle	−1.969	<0.0001	0.0115
10527920	Cyp51	−1.967	0.0012	0.0851
10582879	Csprs	3.771	<0.0001	0.0258
10538126	Gimap4	4.368	0.0052	0.1382
10551025	Cd79a	6.435	0.0018	0.0957
10429520	Ly6d	6.483	0.0028	0.1104
10466172	Ms4a1	7.480	0.0025	0.1050
10392142	Cd79b	7.764	0.0004	0.0552
10458278	Mzb1	9.573	0.0002	0.0469
10523359	Cxcl13	11.166	0.0015	0.0918
10531724	Plac8	11.549	0.0006	0.0634
10429564	Ly6a	12.571	<0.0001	0.0306

[a] Aged versus young peritoneal macrophages; negative fold-change reflects decreased expression in aged macrophages relative to young macrophages.

Table 2
Expression profiling of lipid-related genes in aged and young macrophages.

Cellular function	Gene symbol	Fold change[a]	P-value[b]
Biosynthesis	Fads2	−1.545	0.050
	Fads3	1.299	0.050
	Fdft1	−3.831	0.050
	Fdps	−1.885	0.050
	Hmgcs2	3.122	0.050
	Prkaa2	2.773	0.046
	Scd1	−1.895	0.050
Elimination	Cyp11a1	−9.342	0.050
	Cyp7b1	2.515	0.046
	Cyp27a1	−1.473	0.050
	Hadhb	−1.984	0.050
	Lpl	1.496	0.050
	Tbxas1	1.249	0.050
Leukotriene signaling	Lta4h	−1.314	0.050
	Alox5ap	−1.919	0.050
Transport	Apoa1	−6.985	0.046
	Apof	−6.089	0.050
	Slc16a6	−1.459	0.050
	Slc27a1	−1.659	0.050
	Slc27a3	−4.402	0.050
	Stard4	−1.306	0.050
Uptake	Cxcl16	−1.927	0.050
	Olr1	−2.340	0.050
	Pcsk9	−1.903	0.050
	Stab2	−3.008	0.046
Other or multiple functions	Adfp	2.102	0.050
	Alox15	5.797	0.050
	Fabp4	1.338	0.050
	Nr0b2	−3.911	0.037
	Nr1h3	−1.561	0.050

[a] Aged versus young peritoneal macrophages; negative fold-change reflects decreased expression in aged macrophages relative to young macrophages.
[b] Significant by 2-tailed Mann-Whitney U test.

3.3. Aged Macrophages have Altered Intracellular Oxysterol Content

We previously reported that aged macrophages have higher levels of intracellular cholesterol related to impaired efflux [17], likely related to the global changes in cholesterol homeostatic mechanisms described above. The oxidation of cholesterol to generate oxidized derivatives of cholesterol or oxysterols serves a crucial purpose to facilitate elimination of excess cholesterol. However, oxysterols themselves also play important signaling roles in regulating cholesterol homeostasis [33] and

inflammation [34] and may therefore promote disease. In addition, aberrant oxysterol production can be a sign of increased oxidative stress, which is known to be pathogenic in AMD [35]. Since our transcriptomic profiling demonstrated that impaired cholesterol homeostasis is a hallmark feature of aged macrophages, we sought to explore whether these changes were associated with altered oxysterol signatures, which would not only provide mechanistic insight into why there is impaired cholesterol homeostasis but also identify a potential approach for detecting defective cholesterol homeostasis.
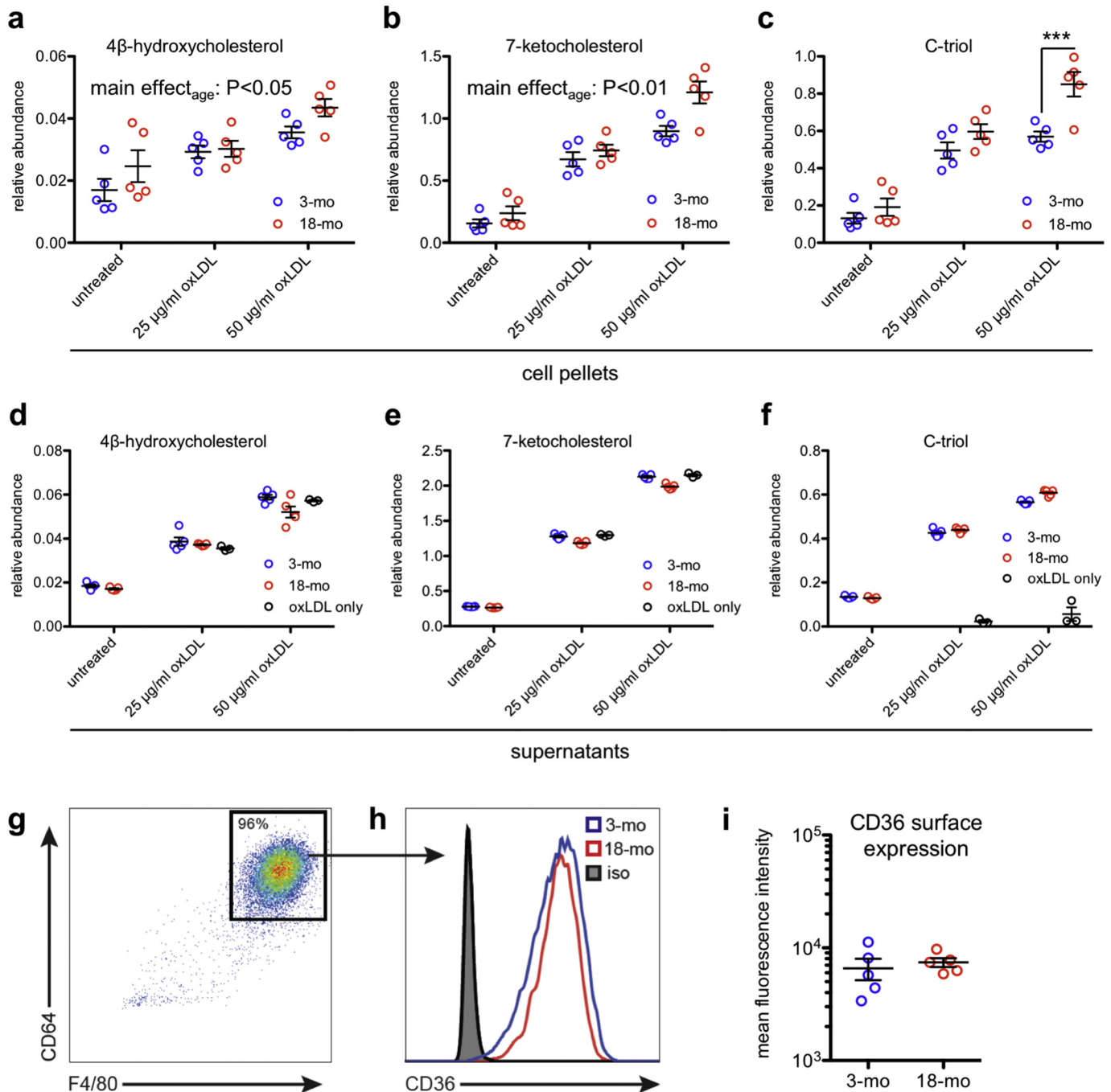

Fig. 3. Aged peritoneal macrophages have abnormal oxysterol content. (a-c) Aged peritoneal macrophages contained significantly more intracellular 4β-hydroxycholesterol (4β-HC) and 7-ketocholesterol (7-KC) than their young counterparts at baseline and after treatment with 25 or 50 μg/ml oxidized LDL (oxLDL) ($N = 5$/group; 2-way ANOVA) and significantly more intracellular cholestane-3β,5α,6β-triol (C-triol) after treatment with 50 μg/ml oxLDL ($N = 5$/group; 2-way ANOVA with Bonferroni post-hoc test). (d-f) Although some comparisons were statistically significant due to low within-group variance, the supernatants of young and aged peritoneal macrophages contained qualitatively similar levels of 4β-HC, 7-KC, and C-triol both at baseline and after treatment with oxLDL ($N = 5$/group; 2-way ANOVA with Bonferroni post-hoc test). (g) Representative flow cytometry plot from young and aged peritoneal macrophages showing gating on macrophage markers CD64 and F4/80. (h-i) Young and aged peritoneal macrophages exhibited similar CD36 surface expression. Isotype staining (iso) was identical between groups ($N = 5$/group; 2-tailed, unpaired t-test). Open circles depict individual data points; horizontal lines depict mean ± SEM (a-f, i) (*** $P < .001$).

Using liquid chromatography tandem mass spectrometry (LC–MS/MS), we measured the most abundant oxysterols, including 4β-hydroxycholesterol (4β-HC), 7-ketocholesterol (7-KC), and cholestane-3β,5α,6β-triol (C-triol) in young and aged peritoneal macrophages. We found that aged peritoneal macrophages contained more 4β-HC and 7-KC compared to young peritoneal macrophages, both at baseline and after treatment with 25 or 50 μg/ml oxidized LDL (oxLDL) (Fig. 3a-b). Aged peritoneal macrophages also had increased C-triol content at baseline and after treatment with oxLDL, but the difference was statistically significant only after treatment with 50 μg/ml oxLDL (Fig. 3c). To account for the possibility that these increases in intracellular oxysterols may have been influenced by environmental factors, we also tested a separate cohort of young and aged mice that were housed at the same animal facility. Consistent with our original findings, these aged peritoneal macrophages also had increased levels of 4β-HC, 7-KC, and C-triol after treatment with 50 μg/ml oxLDL (Fig. S1a–c). These findings demonstrate that aged peritoneal macrophages have increased intracellular oxysterols upon challenge with oxLDL and that this difference is likely an effect of age rather than environmental factors.

We also measured the oxysterol content in the supernatant to determine whether increased intracellular oxysterol content was associated with increased oxysterol secretion. Although some comparisons were statistically significant due to low within-group variance, the levels of 4β-HC, 7-KC, and C-triol were qualitatively similar in the supernatant of both young and aged peritoneal macrophages both at baseline and after treatment with oxLDL (Fig. 3d–f; Fig. S1d–f). Of note, the levels of 4β-HC and 7-KC detected in equivalent dilutions of oxLDL were similar to those detected in the supernatants of both young and aged peritoneal macrophages (Fig. 3d–e; Fig. S1d–e), suggesting that any differences in the secretion of these two oxysterols were likely masked by the oxysterols present in the oxLDL itself.

Our finding of increased intracellular oxysterols in the absence of changes in extracellular levels suggested that there is increased oxysterol synthesis associated with aging rather than changes in uptake. In support of this hypothesis, we previously reported that young and aged macrophages have similar capacity to influx Dil-labeled oxLDL [17]. Furthermore, using flow cytometry, we found that surface expression of CD36, a receptor for oxLDL uptake, was similar in young and aged peritoneal macrophages (Fig. 3g–i), supporting the conclusion that these differences in intracellular oxysterols were not likely due to differences in uptake.

To determine whether these aging-associated changes in oxysterol signatures were specific to elicited peritoneal macrophages, we also measured intracellular oxysterol content and secretion in young and aged splenic macrophages. We found that aged splenic macrophages had similar patterns of increased intracellular oxysterols (Fig. S2a–c) with minimal changes in extracellular oxysterols (Fig. S2d–f). These findings indicate that impaired cholesterol homeostasis is associated with detectable alterations in oxysterol signatures in aged macrophages of multiple origins.

3.4. PBMC and Plasma Oxysterol Signatures are Altered with Age in Humans

We have previously demonstrated that aged murine macrophages exhibit functional shifts that are associated with their tendency to promote AMD [9, 17, 18]. However, it remains unclear which subset of the age-associated changes described above promote disease rather than being a part of physiologic aging. To discriminate between these physiologic versus pathologic changes, we assessed whether PBMCs and plasma samples from healthy human subjects also exhibited changes in oxysterol signatures with age and whether these changes were different in AMD patients. We chose to process the human samples minimally without cell sorting or cultures to explore how these oxysterol signatures could be used clinically. Demographic information of the human subjects is shown in Table 3.

In addition to measuring the same oxysterols we measured in murine peritoneal macrophages (i.e., 4β-HC, 7-KC, and C-triol), we were also able to quantify levels of two additional enzymatically generated oxysterols, 24-hydroxycholesterol (24-HC) and 27-hydroxycholesterol (27-HC), which were below the limit of detection in the murine samples. Of interest, we observed a statistically significant negative correlation between age and PBMC 7-KC levels (Fig. 4a; Spearman $R = -0.2964$, $P = .0204$), PBMC C-triol levels (Fig. 4a; Pearson $R = -0.3068$, $P = .0171$), and PBMC 24-HC levels (Fig. 4b; Pearson $R = -0.3058$, $P = .0165$). There was no association between age and PBMC 4β-HC levels (Fig. 4a; Spearman $R = -0.0356$, $P = .7853$) or PBMC 27-HC levels (Fig. 4b; Pearson $R = -0.0012$, $P = .9930$). Additionally, we observed a significant positive correlation between age and plasma C-triol levels (Fig. 4c; Pearson $R = 0.2818$, $P = .0278$). Although not statistically significant, there was a trend ($0.05 < P < .10$) towards a positive correlation between age and plasma 4β-HC levels (Fig. 4c; Spearman $R = 0.2170$, $P = .0930$). There was no statistically significant correlation between age and plasma 7-KC levels (Fig. 4c; Spearman $R = 0.1172$, $P = .3683$), plasma 24-HC levels (Fig. 4d; Spearman $R = 0.0394$, $P = .7631$), or plasma 27-HC levels (Fig. 4d; Pearson $R = 0.1601$, $P = .2177$). Overall, these findings suggest that healthy humans also exhibit age-associated alterations in oxysterol signatures, likely reflecting changes in cholesterol homeostasis.

3.5. Plasma 24-hydroxycholesterol Distinguishes AMD from Physiologic Aging

To further characterize the relationship between age-associated oxysterol signatures and age-related disease, we recruited human patients with early or advanced neovascular (wet) AMD and measured their PBMC and plasma oxysterol levels (Fig. 5a–j). While AMD patients were significantly older than non-AMD control subjects, there was no difference between the groups on the basis of gender (Table 3). On average, AMD patients had decreased PBMC 7-KC levels compared to non-AMD controls (Fig. 5b) but no differences in the other PBMC oxysterol levels (Fig. 5a/c–e). Moreover, AMD patients had elevated plasma 4β-HC levels (Fig. 5f), elevated plasma C-triol levels (Fig. 5h), elevated plasma 24-HC levels (Fig. 5i), and a trend ($0.05 < P < .10$) towards elevated plasma 27-HC levels (Fig. 5j) compared to non-AMD controls. There was no difference in plasma 7-KC levels (Fig. 5g).

Given the known association between AMD and age and the significant age difference between the two groups, we performed binary logistic regression to precisely model the relationship between PBMC or plasma oxysterol levels and AMD after controlling for age and gender. We selected PBMC 7-KC, plasma 4β-HC, plasma C-triol, and plasma 24-HC levels as candidates for further analysis since these were the oxysterols that were significantly different between AMD patients and controls. The binary logistic regression model for a PBMC oxysterol AMD signature included age, gender, and untransformed PBMC 7-KC (Table 4). The overall model was statistically significant (LR $X^2 = 34.0$, df = 3, $P < .001$) and had good fit ($X^2 = 9.6$, df = 8, $P = .294$). As

Table 3
Demographic and clinical characteristics of human subjects.

Demographic parameter	Control	AMD	P-value
Age, median (range)	64.09 (21.59–87.07)	74.11 (47.87–100.50)	<.0001[a]
Sex, N			
Male	37	23	.3781[b]
Female	25	22	
AMD status, N			
No AMD	62	0	N/A
Early AMD	0	21	
Advanced neovascular AMD	0	24	

[a] Significant by 2-tailed Mann-Whitney U test.
[b] Non-significant by χ^2 test.

expected, age was significantly associated with AMD ($P < .001$) with a beta coefficient of 0.098, indicating that each additional year of age was associated with increased odds of having AMD (aOR = 1.10; 95% CI = 1.05 to 1.16). However, after controlling for age and gender, PBMC 7-KC levels were not associated with AMD ($P = .140$).

The binary logistic regression model for a plasma oxysterol AMD signature included forced entry of age, gender, and any combination of the candidate plasma oxysterol species through automated forward selection (Table 5). The final model was statistically significant (LR $X^2 = $ 44.9, df = 3, $P < .001$), had good fit ($X^2 = 14.2$, df = 8, $P = .078$), and included age, gender, and plasma 24-HC levels. As expected, age was significantly associated with AMD ($P < .001$) with a beta coefficient of 0.107, indicating that each additional year of age was associated with increased odds of having AMD (aOR = 1.113; 95% CI: 1.06 to 1.17). Of significant interest, even after controlling for age and gender, 24-HC levels were highly associated with AMD ($P < .001$) with a beta coefficient of 11.327, indicating that each additional 0.1-unit increase in relative plasma 24-HC levels was associated with a 3.10-fold increase in odds of having AMD (95% CI: 1.66 to 5.79).
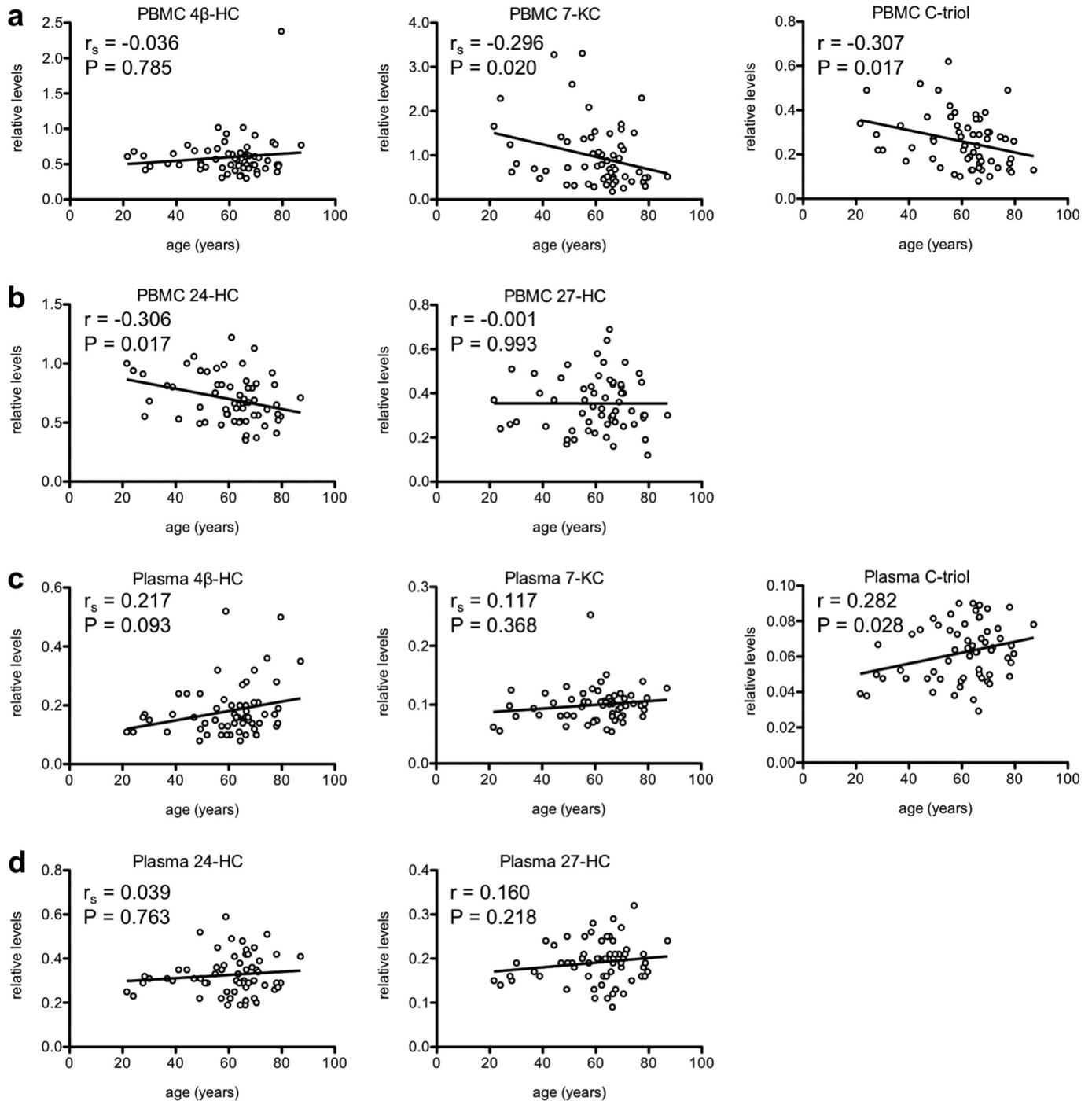

Fig. 4. Age affects human peripheral blood mononuclear cell (PBMC) and plasma oxysterol signatures. (a-b) There was a significant negative correlation between age and PBMC 7-KC levels, PBMC C-triol levels, and PBMC 24-HC levels in healthy human subjects. (c-d) There was a significant positive correlation between age and plasma C-triol levels and a trend towards a positive correlation between age and plasma 4β-HC levels. Open circles depict individual data points; lines depict the best-fitting linear regression line (a-d; r = Pearson product-moment correlation coefficient; r_s = Spearman rank-order correlation coefficient).

Furthermore, we performed conjunctive analysis to evaluate the clinical utility of using plasma 24-HC to discriminate between AMD patients and non-AMD subjects across varying ages. We divided patients into tertiles by plasma 24-HC levels and by age (i.e., above versus below median), tabulating the AMD prevalence in each conjoined cell (Table 6). This analysis demonstrated a clear stepwise increase in prevalence of AMD in subjects above the median age going from the lowest to the highest tertile of plasma 24-HC (i.e., from 47.1% to 66.7% to 76.2%; Fig. 6a). We observed a similar increase in AMD prevalence in subjects below the median age based on plasma 24-HC tertile (i.e., from 10.5% to 19.0% to 38.5%). These findings support the notion that plasma 24-HC levels can distinguish between the changes in cholesterol homeostasis expected during physiologic aging versus those that suggest risk of

AMD. To determine the efficacy of plasma 24-HC levels as a potential marker for AMD, we generated a receiver operating characteristic (ROC) curve and found that the area under the ROC curve (AUC) was 0.866 (95% CI: 0.793 to 0.939), indicating good discrimination (Fig. 6b).

To determine the clinical utility of plasma 24-HC levels compared to existing clinical measures of lipid homeostasis, we next analyzed whether plasma 24-HC levels were correlated with total plasma cholesterol levels in the subjects for whom this information was available. In these subjects ($N = 37$), plasma 24-HC was indeed correlated with total plasma cholesterol ($R = 0.659$, $P < .001$). We therefore performed a subanalysis by generating a binary logistic regression for the outcome of AMD with forced entry of plasma 24-HC levels, total plasma cholesterol, age, and gender. This model was statistically significant (LR X^2
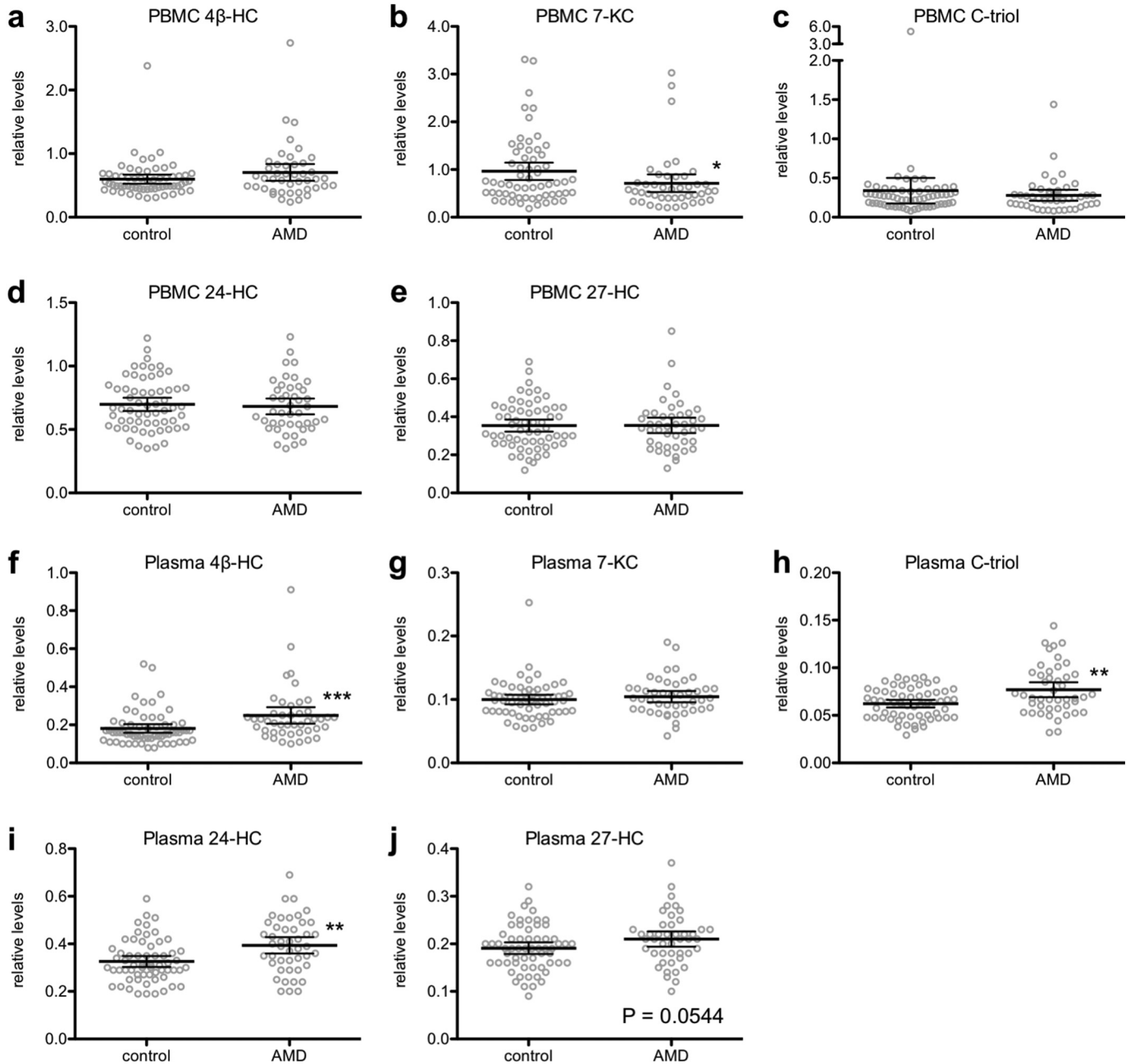

Fig. 5. Age-related macular degeneration (AMD) patients have altered peripheral blood mononuclear cell (PBMC) and plasma oxysterol signatures. (a-j) We measured PBMC and plasma levels of 4β-HC, 7-KC, C-triol, 24-HC, and 27-HC. AMD patients ($N = 44$–45) had decreased PBMC 7-KC levels (b; 2-tailed Mann-Whitney U test), elevated plasma 4β-HC levels (f; 2-tailed Mann-Whitney U test), elevated plasma C-triol levels (h; 2-tailed Mann-Whitney U test), elevated plasma 24-HC levels (i; 2-tailed Mann-Whitney U test), and a trend towards elevated plasma 27-HC levels (j; 2-tailed, unpaired t-test) compared to non-AMD controls ($N = 61$). Open circles depict individual data points; horizontal lines depict mean ± 95% confidence intervals (a-j) (* $P < .05$; ** $P < .01$; *** $P < .001$).

$= 27.2, \mathrm{df} = 4, P < .001$) and had good fit ($X^2 = 2.6, \mathrm{df} = 7, P = .921$). Of interest, total plasma cholesterol levels were not associated with AMD (aOR = 1.014; 95% CI: 0.97 to 1.06; $P = .547$). Remarkably, even after controlling for total plasma cholesterol, age, and gender, plasma 24-HC remained associated with AMD ($P = .044$) with a beta coefficient of 19.308, indicating that each additional 0.1-unit increase in relative plasma 24-HC levels was associated with a 6.90-fold increase in odds of having AMD (95% CI: 1.05 to 45.09). Despite the limited sample size available for this subanalysis, these findings suggest that human plasma 24-HC has strong diagnostic value compared to the existing measure of total plasma cholesterol.

Given the heterogeneity of the clinical progression of AMD and our interest in identifying factors that may predict transition to advanced disease, we also examined whether plasma 24-HC levels differed significantly when subdividing AMD patients into early AMD and advanced neovascular AMD patients. We did not detect a statistically significant difference in plasma 24-HC levels in early AMD versus advanced neovascular AMD patients (Fig. 6c). Therefore, although 24-HC may be associated with AMD, it does not appear to have utility for predicting disease progression based on this cross-sectional analysis.

4. Discussion

In this study, we identified that despite their self-renewal, macrophages from old mice exhibit signs of aging, such as defects in mitochondrial oxidative respiration, that are not observed in macrophages from young mice. Consistent with these functional changes, aged macrophages exhibit an altered transcriptomic profile, especially in genes involved in cholesterol homeostasis. These findings build on our previous study reporting that *Abca1* expression is significantly reduced in aged macrophages, leading to impaired cholesterol efflux [17]. We further demonstrate that impairments in cholesterol homeostatic mechanisms are not restricted solely to efflux but globally affect myriad pathways, including biosynthesis, elimination, transport, and regulation. Interestingly, aged macrophages exhibited simultaneous downregulation and upregulation of different genes having similar functions in cholesterol-related pathways (Table 2), indicating broad and complex dysregulation of cholesterol homeostasis.

Our hypothesis that impaired cholesterol metabolism in aged macrophages contributes to AMD pathogenesis is consistent with numerous epidemiological studies that have established that parameters related to lipid status, such as baseline high-density lipoprotein-cholesterol (HDL-C) and total serum cholesterol, affect risk of AMD development and progression [36–38]. Moreover, one past genome-wide association study reported that polymorphisms in lipid-related genes such as LIPC, ABCA1, and CETP are associated with advanced AMD [20]. These findings have led to the hypothesis that statins, cholesterol-lowering drugs used for cardiovascular disease, may affect the development or progression of AMD [39]. The findings of one non-randomized study suggest that high-dose statins may indeed reduce some high-risk features of AMD [40], although large randomized studies are necessary to confirm these findings [41] given that numerous other studies report conflicting results [42]. Cumulatively, these conflicting findings highlight that the relationship between aging, impaired cholesterol homeostasis, and AMD is complex and warrants further investigation.

In this study, we found that in aged murine macrophages, a transcriptomic profile suggesting impaired cholesterol homeostasis was associated with aberrant intracellular oxysterol levels, especially

when the macrophages were treated with oxLDL. In many immune cells, oxysterols can directly regulate liver X receptor (LXR) transcriptional activity, which can modulate cellular lipid metabolism and the immune response, especially in inflammation-associated diseases [33]. For example, 27-HC, the most prevalent oxysterol in atherosclerotic lesions, has been shown to promote atherosclerosis by inducing inflammation [43]. Therefore, in addition to being a surrogate marker for impaired cholesterol homeostasis, altered oxysterol production may itself play a pathogenic role in promoting cholesterol dysregulation. Further studies are necessary to uncover the mechanisms underlying altered oxysterol content, which may be related to altered uptake or synthesis. However, our results broadly suggest that altered oxysterols in macrophages are markers of cholesterol dyshomeostasis.

We found that, similar to murine macrophages, human PBMC and plasma samples demonstrated age-dependent and disease-dependent changes in oxysterols. Although the directionality of these changes did not correspond perfectly between mice and humans, our data suggest that broad dysregulation of cholesterol homeostasis in both aging and disease is associated with altered oxysterol signatures. These findings build on recent reports that monocytes isolated from patients with neovascular AMD do indeed exhibit an altered immune-related transcriptomic signature [44] and that these cells, when activated into macrophages, demonstrate proangiogenic characteristics that may contribute to disease pathogenesis [45]. Past studies have also shown that in the outer retina, accumulation of cholesterol oxidation products such as 7-KC can disrupt the immune environment and transform resident macrophages into disease-promoting cells [46]. Specifically, uptake of 7-KC in microglial cells results in decreased production of neurotrophic growth factors and increased expression of angiogenic mediators that promote pathologic CNV [46]. Although there are likely some differences between the mechanisms of altered oxysterols in mice and humans, our work support the broad idea that oxysterols can be used to identify features of cholesterol dyshomeostasis.

How to distinguish whether changes in oxysterol signatures define aging, disease, or both is of great interest, as defects in lipid metabolism are a shared feature of multiple diseases. As an example, certain oxysterols and their metabolites have been shown to be specific biomarkers for Niemann-Pick type C (NPC) disease, an inherited lysosomal storage disease [47, 48]. In this study, we found that after controlling for age and gender, plasma 24-HC was significantly associated with AMD. Despite our modest sample size ($N = 107$), these findings suggest that 24-HC is a strong candidate for an oxysterol that distinguishes AMD from physiologic aging. Although limited by sample size and therefore a relatively wide confidence interval, our subanalysis revealed that plasma 24-HC remained associated with AMD even after controlling for total plasma cholesterol, highlighting its diagnostic value. Larger prospective studies are necessary to validate these findings and identify additional markers of risk.

Table 4
Beta coefficients from PBMC binary logistic regression model.

Predictor variable	aOR (e^β)	95% CI of e^β	P-value
Age	1.103	1.049 to 1.161	<0.001
Female gender	0.893	0.335 to 2.381	0.821
PBMC 7-KC levels, 1-unit	0.351	0.087 to 1.412	0.140

Table 5
Beta coefficients from plasma binary logistic regression model.

Predictor variable	aOR (e^β)	95% CI of e^β	P-value
Age	1.113	1.055 to 1.174	<0.001
Female gender	0.390	0.119 to 1.282	0.121
Plasma 24-HC levels, 0.1-unit	3.104	1.66 to 5.79	<0.001

Table 6
AMD as a function of age and plasma 24-HC levels.

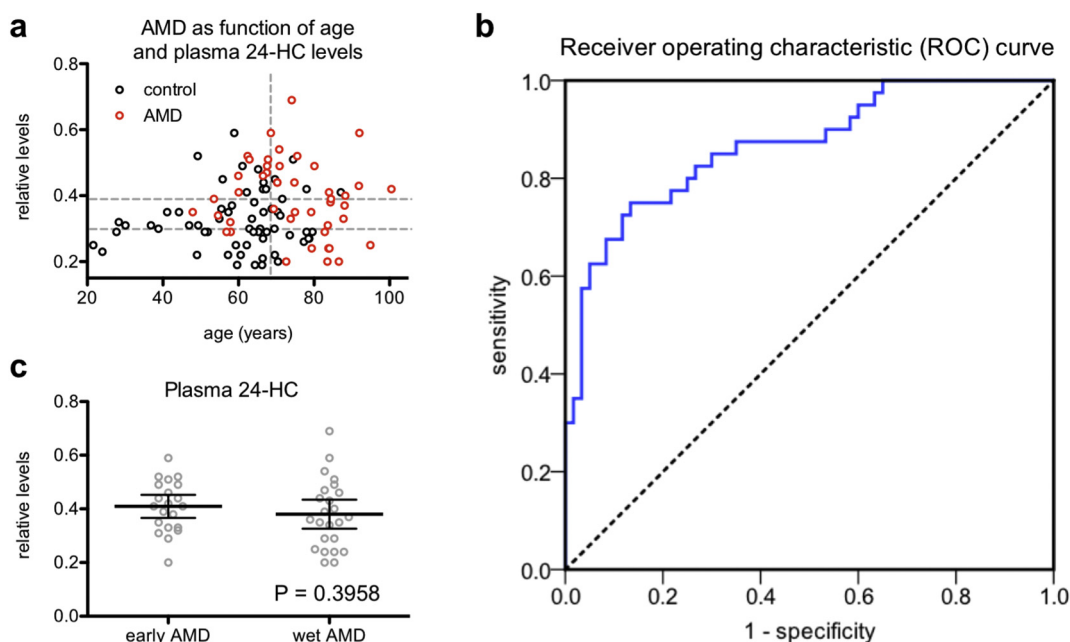|		Age		
		Below median	Above median	Total
Plasma 24-HC	Lowest tertile	2/19 (10.5%)	8/17 (47.1%)	10/36 (27.8%)
	Middle tertile	4/21 (19.0%)	10/15 (66.7%)	14/36 (38.9%)
	Highest tertile	5/13 (38.5%)	16/21 (76.2%)	21/34 (61.8%)
	Total	11/53 (20.8%)	34/53 (64.2%)	45/106 (42.5%)

Fig. 6. Plasma 24-HC levels discriminate age-related macular degeneration (AMD) from physiologic aging. (a) We divided patients into tertiles by plasma 24-HC and by age (i.e., above versus below median age) and found that individuals in the highest tertile of plasma 24-HC who were also above median age (top right) had the highest AMD prevalence. Horizontal dashed grey lines demarcate plasma 24-HC tertiles; the vertical dashed grey line indicates the median age. (b) Receiver operating characteristic (ROC) curve showing plasma 24-HC discriminates between AMD patients and control subjects. (c) We did not observe a statistically significant difference in plasma 24-HC levels in early AMD patients versus advanced neovascular (wet) AMD patients ($N = 21$ early AMD; 24 wet AMD; 2-tailed, unpaired t-test). Open circles depict individual data points (a, c); horizontal lines depict mean $\pm$ 95% confidence intervals (c).

Cumulatively, our findings highlight that impaired cholesterol homeostasis is a key pathway perturbed in aged macrophages and that oxysterol signatures in patient samples can distinguish AMD from physiologic aging. Ultimately, these findings may not only improve our ability to diagnose disease but also identify targets in cholesterol homeostasis pathways for novel therapeutic approaches.

Declaration of Interests

The authors declare that no conflict of interest exists.

Author Contributions

A. Sene performed most of the experiments related to Figs 1–2; J.B.L. performed most of the experiments related to Figs 3–6.
Conceptualization: R.S.A., A. Sene, J.B.L.
Investigation: J.B.L., A. Sene, A. Santeford, H.F., R.S., M.M.L., V.A.S., N.B.
Writing – Original Draft: J.B.L., A. Sene
Writing – Review & Editing: J.B.L., A. Sene, R.S.A., D.S.O., N.B., M.M.L., H.F., V.A.S.
Supervision: R.S.A., D.S.O., I.U.M.
Funding Acquisition: R.S.A., D.S.O., I.U.M.

Appendix A. Supplementary data

Supplementary data to this article can be found online at https://doi.org/10.1016/j.ebiom.2018.05.035.

References

[1] van Leeuwen R, Klaver CC, Vingerling JR, Hofman A, de Jong PT. Epidemiology of age-related maculopathy: a review. Eur J Epidemiol 2003;18(9):845–54.
[2] Ferris 3rd FL, Fine SL, Hyman L. Age-related macular degeneration and blindness due to neovascular maculopathy. Arch Ophthalmol 1984;102(11):1640–2 Chicago, Ill: 1960.
[3] Sarwar S, Clearfield E, Soliman MK, et al. Aflibercept for neovascular age-related macular degeneration. Cochrane Database Syst Rev 2016;2:Cd011346.
[4] Kim JH, Lee DW, Chang YS, Kim JW, Kim CG. Twelve-month outcomes of treatment using ranibizumab or aflibercept for neovascular age-related macular degeneration: a comparative study. Graefe's archive for clinical and experimental ophthalmology = Albrecht von Graefes Archiv fur klinische und experimentelle. Fortschr Ophthalmol 2016;254(11):2101–9.

[5] Inoue M, Yamane S, Sato S, Sakamaki K, Arakawa A, Kadonosono K. Comparison of time to retreatment and visual function between Ranibizumab and Aflibercept in age-related macular degeneration. Am J Ophthalmol 2016;169:95–103.

[6] Haller JA. Current anti-vascular endothelial growth factor dosing regimens: benefits and burden. Ophthalmology 2013;120(5 Suppl):S3–7.

[7] Zinkernagel MS, Schorno P, Ebneter A, Wolf S. Scleral thinning after repeated intra-vitreal injections of antivascular endothelial growth factor agents in the same quadrant. Invest Ophthalmol Vis Sci 2015;56(3):1894–900.

[8] Sene A, Chin-Yee D, Apte RS. Seeing through VEGF: innate and adaptive immunity in pathological angiogenesis in the eye. Trends Mol Med 2015;21(1):43–51.

[9] Apte RS, Richter J, Herndon J, Ferguson TA. Macrophages inhibit neovascularization in a murine model of age-related macular degeneration. PLoS Med 2006;3(8):e310.

[10] Espinosa-Heidmann DG, Suner IJ, Hernandez EP, Monroy D, Csaky KG, Cousins SW. Macrophage depletion diminishes lesion size and severity in experimental choroidal neovascularization. Invest Ophthalmol Vis Sci 2003;44(8):3586–92.

[11] Sakurai E, Anand A, Ambati BK, van Rooijen N, Ambati J. Macrophage depletion inhibits experimental choroidal neovascularization. Invest Ophthalmol Vis Sci 2003; 44(8):3578–85.

[12] Lin JB, Moolani HV, Sene A, et al. Macrophage microRNA-150 promotes pathological angiogenesis as seen in age-related macular degeneration. JCI Insight 2018;3(7).

[13] Mosser DM, Edwards JP. Exploring the full spectrum of macrophage activation. Nat Rev Immunol 2008;8(12):958–69.

[14] Sica A, Mantovani A. Macrophage plasticity and polarization: in vivo veritas. J Clin Invest 2012;122(3):787–95.

[15] Murray PJ, Allen JE, Biswas SK, et al. Macrophage activation and polarization: nomenclature and experimental guidelines. Immunity 2014;41(1):14–20.

[16] Kelly J, Ali Khan A, Yin J, Ferguson TA, Apte RS. Senescence regulates macrophage activation and angiogenic fate at sites of tissue injury in mice. J Clin Invest 2007;117 (11):3421–6.

[17] Sene A, Khan AA, Cox D, et al. Impaired cholesterol efflux in senescent macrophages promotes age-related macular degeneration. Cell Metab 2013;17(4):549–61.

[18] Nakamura R, Sene A, Santeford A, et al. IL10-driven STAT3 signalling in senescent macrophages promotes pathological eye angiogenesis. Nat Commun 2015;6:7847.

[19] Sene A, Apte RS. Eyeballing cholesterol efflux and macrophage function in disease pathogenesis. Trends Endocrinol Metab TEM 2014;25(3):107–14.

[20] Neale BM, Fagerness J, Reynolds R, et al. Genome-wide association study of advanced age-related macular degeneration identifies a role of the hepatic lipase gene (LIPC). Proc Natl Acad Sci U S A 2010;107(16):7395–400.

[21] Ferris FL, Davis MD, Clemons TE, et al. A simplified severity scale for age-related macular degeneration: AREDS report no. 18. Arch Ophthalmol 2005;123(11): 1570–4 Chicago, Ill: 1960.

[22] Faul F, Erdfelder E, Lang AG, Buchner A. G*power 3: a flexible statistical power analysis program for the social, behavioral, and biomedical sciences. Behav Res Methods 2007;39(2):175–91.

[23] Jiang X, Sidhu R, Porter FD, et al. A sensitive and specific LC–MS/MS method for rapid diagnosis of Niemann-pick C1 disease from human plasma. J Lipid Res 2011;52(7): 1435–45.

[24] Hashimoto D, Chow A, Noizat C, et al. Tissue-resident macrophages self-maintain locally throughout adult life with minimal contribution from circulating monocytes. Immunity 2013;38(4):792–804.

[25] Lopez-Otin C, Blasco MA, Partridge L, Serrano M, Kroemer G. The hallmarks of aging. Cell 2013;153(6):1194–217.

[26] Tavakoli S, Zamora D, Ullevig S, Asmis R. Bioenergetic profiles diverge during macrophage polarization: implications for the interpretation of 18F-FDG PET imaging of atherosclerosis. J Nucl Med 2013;54(9):1661–7.

[27] Vats D, Mukundan L, Odegaard JI, et al. Oxidative metabolism and PGC-1beta attenuate macrophage-mediated inflammation. Cell Metab 2006;4(1):13–24.

[28] Huang SC, Everts B, Ivanova Y, et al. Cell-intrinsic lysosomal lipolysis is essential for alternative activation of macrophages. Nat Immunol 2014;15(9):846–55.

[29] Randle DH, Zindy F, Sherr CJ, Roussel MF. Differential effects of p19Arf and p16Ink4a loss on senescence of murine bone marrow-derived preB cells and macrophages. Proc Natl Acad Sci 2001;98(17):9654–9.

[30] Nielsen GP, Stemmer-Rachamimov AO, Shaw J, Roy JE, Koh J, Louis DN. Immunohistochemical survey of p16INK4A expression in normal human adult and infant tissues. Lab Invest 1999;79(9):1137–43.

[31] Zindy F, Quelle DE, Roussel MF, Sherr CJ. Expression of the p16INK4a tumor suppressor versus other INK4 family members during mouse development and aging. Oncogene 1997;15(2):203–11.

[32] Krishnamurthy J, Torrice C, Ramsey MR, et al. Ink4a/Arf expression is a biomarker of aging. J Clin Invest 2004;114(9):1299–307.

[33] Spann NJ, Glass CK. Sterols and oxysterols in immune cell function. Nat Immunol 2013;14(9):893–900.

[34] Poli G, Biasi F, Leonarduzzi G. Oxysterols in the pathogenesis of major chronic diseases. Redox Biol 2013;1:125–30.

[35] Datta S, Cano M, Ebrahimi K, Wang L, Handa JT. The impact of oxidative stress and inflammation on RPE degeneration in non-neovascular AMD. Prog Retin Eye Res 2017;60:201–2018.

[36] Tomany SC, Wang JJ, Van Leeuwen R, et al. Risk factors for incident age-related macular degeneration: pooled findings from 3 continents. Ophthalmology 2004;111(7): 1280–7.

[37] Yip JL, Khawaja AP, Chan MP, et al. Cross sectional and longitudinal associations between cardiovascular risk factors and age related macular degeneration in the EPIC-Norfolk eye study. PLoS One 2015;10(7):e0132565.

[38] Burgess S, Davey Smith G. Mendelian randomization implicates high-density lipoprotein cholesterol-associated mechanisms in etiology of age-related macular degeneration. Ophthalmology 2017;124(8):1165–74.

[39] Hall NF, Gale CR, Syddall H, Phillips DI, Martyn CN. Risk of macular degeneration in users of statins: cross sectional study. BMJ (Clin Res Ed) 2001;323(7309):375–6.

[40] Vavvas DG, Daniels AB, Kapsala ZG, et al. Regression of some high-risk features of age-related macular degeneration (AMD) in patients receiving intensive statin treatment. EBioMedicine 2016;5:198–203.

[41] Apte RS. Targeting tissue lipids in age-related macular degeneration. EBioMedicine 2016;5:26–7.

[42] Gehlbach P, Li T, Hatef E. Statins for age-related macular degeneration. Cochrane Database Syst Rev 2016(8):Cd006927.

[43] Umetani M, Ghosh P, Ishikawa T, et al. The cholesterol metabolite 27-hydroxycholesterol promotes atherosclerosis via proinflammatory processes mediated by estrogen receptor alpha. Cell Metab 2014;20(1):172–82.

[44] Grunin M, Hagbi-Levi S, Rinsky B, Smith Y, Chowers I. Transcriptome analysis on monocytes from patients with Neovascular age-related macular degeneration. Sci Rep 2016;6:29046.

[45] Hagbi-Levi S, Grunin M, Jaouni T, et al. Proangiogenic characteristics of activated macrophages from patients with age-related macular degeneration. Neurobiol Aging 2017;51:71–82.

[46] Indaram M, Ma W, Zhao L, Fariss RN, Rodriguez IR, Wong WT. 7-Ketocholesterol increases retinal microglial migration, activation, and angiogenicity: a potential pathogenic mechanism underlying age-related macular degeneration. Sci Rep 2015;5: 9144.

[47] Jiang X, Sidhu R, Mydock-McGrane L, et al. Development of a bile acid-based newborn screen for Niemann-pick disease type C. Sci Transl Med 2016;8(337):337ra63.

[48] Porter FD, Scherrer DE, Lanier MH, et al. Cholesterol oxidation products are sensitive and specific blood-based biomarkers for Niemann-pick C1 disease. Sci Transl Med 2010;2(56):56ra81.